Modeling Slag Deposition in the Space Shuttle Solid Rocket Motor

S. Boraas*
Morton Thiokol, Inc., Brigham City, Utah

The burning of an aluminized propellant within a solid rocket motor produces liquid Al/Al_2O_3 droplets on the propellant surface. Upon leaving the surface and experiencing collisions with other droplets large agglomerates may form. A significant percentage of these droplets and/or agglomerates may be deposited on the inner surfaces of the motor as a consequence of their inability to follow the gas streamlines through the nozzle. The study described herein develops an understanding of this deposition process through flow modeling and the subsequent accumulation and pooling of this slag material within the Space Shuttle solid rocket motor (SRM). From this, an analytical procedure was developed for predicting certain unknowns relating to the deposition and pooling processes. The results of an analysis using this procedure have been qualitatively verified by post-test observations of solidified slag within static horizontally fired motors. The results of the analysis were used to provide an explanation for the slag in the QM-2 and to predict the effects of flight acceleration on slag formation. The procedure is applicable to any rocket motor configuration, although IS was devloped for the SRM.

Nomenclature

d	= droplet diameter
$d'_{\min}$	= minimum droplet diameter
D	= pooled slag depth (Fig. 12)
f	= mass fraction of Al_2O_3
F_v	= droplet volume fraction (Fig. 8)
K	= gas turning loss coefficient for angle ϕ
L	= pooled slag length (Fig. 12)
P_0	= chamber gas pressure
q	= flow dynamic pressure
r	= radial location of droplet
R^*	= nozzle throat radius
t	= burn time
t_c	= time when critical slag depth occurs
t_p	= slag pooling time
t'	= slag deposition time
T_0	= chamber gas temperature
v	= volume of pooled slag
$\dot{w}$	= flow rate
W_s	= slag weight
x	= axial location of droplet
y_w	= wall contour coordinate (Fig. 12)
θ	= meridonal angle (Fig. 11)
ρ	= slag density
ϕ	= flow turning angle (Fig. 12)

Subscripts

c	= critical
d	= deposited
e	= escaped
s	= slag
tot	= total
max	= maximum
min	= minimum
av	= average
AV	= time average of average values

Submitted June 16, 1982; presented as Paper 82-1061 at the AIAA/SAE/ASME 18th Joint Propulsion Conference, Cleveland, Ohio, June 21-23, 1982; revision received July 26, 1983.

*Associate Scientist, Motor Performance, Wasatch Division. Member AIAA.

I. Introduction

THE combustion of an aluminized solid propellant produces Al/Al_2O_3 liquid droplets on the burning propellant surface. These droplets are the source of a slag-like material that may remain in the motor during a firing and will contribute to a motor performance loss and possible damage to surfaces where it collects as a result of excessive heating. Although the subject of aluminized propellant combustion and droplet formation has received a certain amount of attention recently, the nature and extent of their deposition once the droplets leave the burning surfaces is not well known.[1-5] The purpose of this study was to develop through flow modeling a better understanding of this process within the solid rocket motor (SRM) so that an analytical procedure could be developed for evaluating particular unknowns relating to this deposition. Through analysis, it was demonstrated that the evaluation of these unknowns not only provided a better insight into the subsequent localized accumulation of deposited droplets, but also into the pooling of this collected material during a static horizontal motor firing.

The results of the analysis showed that the origin of the slag was droplets extracted from the outer annular region of the gas flowfield. Due to the severe turning required by the streamlines in this region at the nozzle entrance, the droplets deposited from this region impinge upon the outer surface of the submerged nozzle and the adjacent motor case wall. It was postulated that the slag accumulation on these surfaces leads to pooling of the slag within the recirculation region caused by the nozzle submergence. Post-test observations of solidified slag formed during static SRM firings have verified these deposition, accumulation, and pooling processes.

The results of the analysis propellant differences. They also indicated that during flight, the axial acceleration on the SRM will probably not increase the amount of slag deposited above that encountered during static tests.

The analytical procedure was developed specifically for the SRM, which has a large length-to-diameter ratio and a center-perforated grain. Although applicable to all configurations, departure from this general configuration may make an analysis somewhat more complicated.

II. Technical Development

The purpose of this study was to develop an analytical procedure for evaluating certain unknowns relating to slag

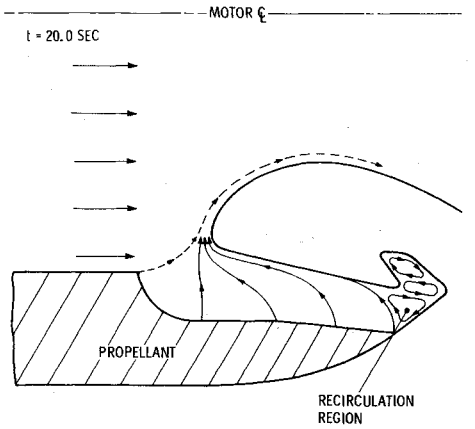

Fig. 1 Flow in the submerged nozzle region near the start of the burn.

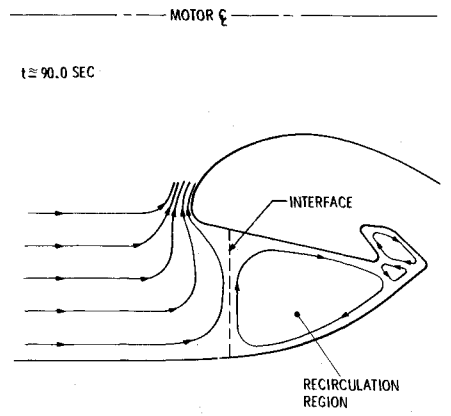

Fig. 2 Flow in the submerged nozzle region near the end of the burn.

deposition within the SRM. The development was based upon an intuitive determination of the time during the motor burn when conditions for slag deposition were most favorable. It also required the definition of a model which is representative of the gas-droplet flowfield during this deposition period. Having determined these, the data required for a deposition analysis were generated and then the analysis was conducted.

The results of the deposition analysis led to a hypothesis concerning the nature of slag deposition and its accumulation. This in turn suggested a hypothesis regarding slag pooling in the nozzle region. The latter became the basis for developing an expression for the maximum slag depth during a static horizontal motor firing. All these aspects of slag modeling, which are described in detail in Ref. 6, are discussed in the following paragraphs.

Deposition Process

The two essential requirements for understanding the deposition process are the approximate time period when it occurs and a model which is representative of the two-phase flow during this period. This model is used to determine the maximum size droplets that can escape the chamber during the time deposition takes place.

Figure 1 shows the location of the propellant surface relative to the submerged nozzle early in the burn. This flow schematic represents an unfavorable situation for droplet distribution, since a large fraction of the droplets outside the bounds of a cylinder, whose radius is equal to that of the nozzle throat, would normally impinge on the nozzle surface were it not for the sweeping action of the crossflow emanating from the propellant underneath the nozzle. Figure 2 shows the corresponding conditions near the end of the motor burn when not only is there a larger percentage of droplets outside the cylinder, but the sweeping action is no longer present. Consequently, it was postulated that deposition takes place near the end of the motor burn.

The two-phase (gas, droplet) flowfield during the deposition period may be envisioned as coming into existence in the following manner. Liquid droplets of Al/Al_2O_3 which form on the burning propellant surface will be swept off the surface and driven downstream by the drag forces generated by the oncoming combustion gases. In the SRM, the droplets will continue to burn during their passage down the length of the chamber, since a chemical analysis of the deposited slag material indicated essentially no free aluminum. In addition to burning, collisions and coalescence with other droplets will take place. The result is the establishment of a large-size distribution, varying from individual droplets to large agglomerates, by the time the nozzle entrance is reached. This distribution is assumed to be uniform across the chamber at the nozzle entrance. This should be a reasonable asumption for the SRM, where the burning propellant surface has receded far forward of the nozzle entrance by the time deposition is expected to take place. As noted, this distribution will consist of individual droplets and agglomerates. For the sake of convenience, in the ramainder of this paper "droplet" will mean a single droplet or an agglomerate of droplets.

The probability that a droplet escapes from the chamber rather than being deposited depends upon its tendency to follow a gas streamline through the nozzle. In terms of the gas flowfield at the nozzle, it means that the greater the turning required by a gas streamline, the smaller a droplet must be on it if it is to escape. Figure 3 is a schematic of the relative size distribution of the escaping droplets approaching the nozzle on streamlines representing various percentages of the total gas flow. It shows, for example, that the escaping droplet on the 60% gas flow streamline is larger than the one on the 90% gas flow streamline since the latter pursues a more tortuous path. The 37.5% gas flow streamline represents for the SRM the bounds of a cylinder whose radius is that of the nozzle throat. It represents an escape zone, since all droplets within this cylinder (regardless of size) will escape.

The above-described flow model shows that the smaller droplets approaching the nozzle generally will be expelled and that all droplets within the escape zone, regardless of size, will escape. There will be larger droplets outside of this zone which are within the inner region of the chamber and as a result will not undergo extreme deviations from their lineal paths of approach to the nozzle. These droplets may also escape only to experience possible breakup in the throat due to shear forces.[2] However, a significant percentage of the droplets in the outer region of the chamber will be deposited on the inner surfaces of the motor since they lack an inclination to follow the rapidly turning gas streamlines.

The turning required by the streamlines in the outer region depends upon the size of the recirculation region: therefore its size must be determined. This could have been done mathematically using an existing adaptation[7] of the SOLA code.[8] The approach taken in this study consisted of determining the location of the interface between the flowing gas and the recirculation region from momentum considerations[6] and correcting the computed values of this location using the cold flow data of Ref. 9.

Required Data

The procedure for calculating the unknown quantities relating to deposition was based upon results from the following studies:

1) Droplet trajectory calculations[6] using a computer program to calculate the maximum size of the escaping droplet as a function of its radical position within the flowfield.

2) A slag flow analysis using results from a thermochemical program[10] leading to information relating slag weight to deposition time and rate.

3) An earlier experimental study[1] to determine droplet size distribution near the burning surface of an aluminized propellant using high-speed photography.

Droplet Trajectory Results

A droplet trajectory program was used to calculate the trajectory of the droplets traversing the length of the SRM chamber. These calculations were made for a static horizontal motor firing using spin acceleration to simulate the gravitational effect on a droplet at a given radial location.

The droplet trajectory calculations determined the maximum droplet size capable of being swept out of the nozzle for a given set of the following variables: 1) burn time; 2) initial axial location of the droplet; 3) initial radial location of the droplet; 4) droplet diameter; 5) initial velocity lag; and 6) initial temperature lag.

To simplify the scope of the calculations, the effects of velocity and temperature lags were neglected. Some preliminary studies had already indicated that velocity lag would have virtually no effect on the trajectory of droplets less than 80 μm in diameter. Because it was expected that the size of the droplets comprising the deposited slag would be less than 80 μm, the effect of velocity lag was neglected. The effect of temperature lag was expected to be even less, hence its neglect also seemed justified. Thus only four parameters (t, x, r, d) were varied in the droplet trajectory studies. This was done by selecting a burn time and an initial droplet location and then varying the droplet diameter until the maximum diameter (d_{max}) of an escaping droplet was found.

Having theorized that the deposition takes place primarily during the end of the burn, the three times (97.34, 111.0, and 120.0 s) selected represent the times near the start of the shutdown, near the end of the shutdown, and an intermediate value. Three axial locations (976.4, 1114.4, and 1214.2 in.) and seven radial locations (40, 60, 90, 92, 94, 96, and 98% gas flow streamlines) were chosen and droplet diameters were varied from 1 to 1200 μm. The reference axial location ($x=0$) was the leading edge of the forward motor segment.

Combinations of these variables resulted in several hundred trajectory calculations. It was found that for conditions near the end of the motor burn d_{max} is independent of the initial axial location of the droplet and is also independent of the burn time between 97.34 and 111.0 s. This independence of d_{max} on both the initial axial location and the burn time greatly simplified the subsequent analysis. It is largely due to the large length-to-diameter ratio of the SRM and its simple, center-perforated grain design. For other motor configurations, where this is not the case, the results may show a dependence on these variables. The results of the trajectory calculations, which are plotted in Fig. 4, show that the maximum droplet size has been reduced primarily to a dependancy on its initial radial position.

Slag Flow Analysis

The total slag flow rate through the SRM was calculated as a function of time prior to an during the shutdown period using the recorded chamber pressures P_0 from the second qualification motor (QM-2) firing. Table 1 shows the calculated flow conditions within the QM-2 during the period from 97.34 to 123.07 s when the chamber pressure reaches the Utah ambient value of about 13 psi. With the measured values of chamber pressure, the combustion temperatures and the mass fractions of the liquid Al_2O_3 were obtained from a thermochemical analysis of the flowfield. The total slag flow rate, which is the product of the total mass flow rate and the mass fraction, is shown plotted in Fig. 5 as a function of time into the burn.

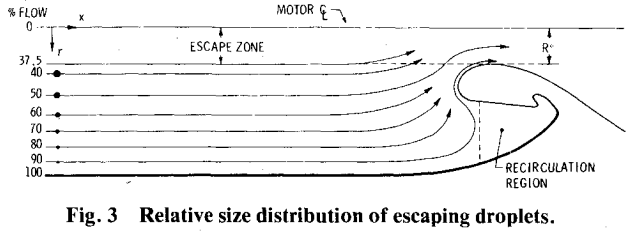

Fig. 3 Relative size distribution of escaping droplets.

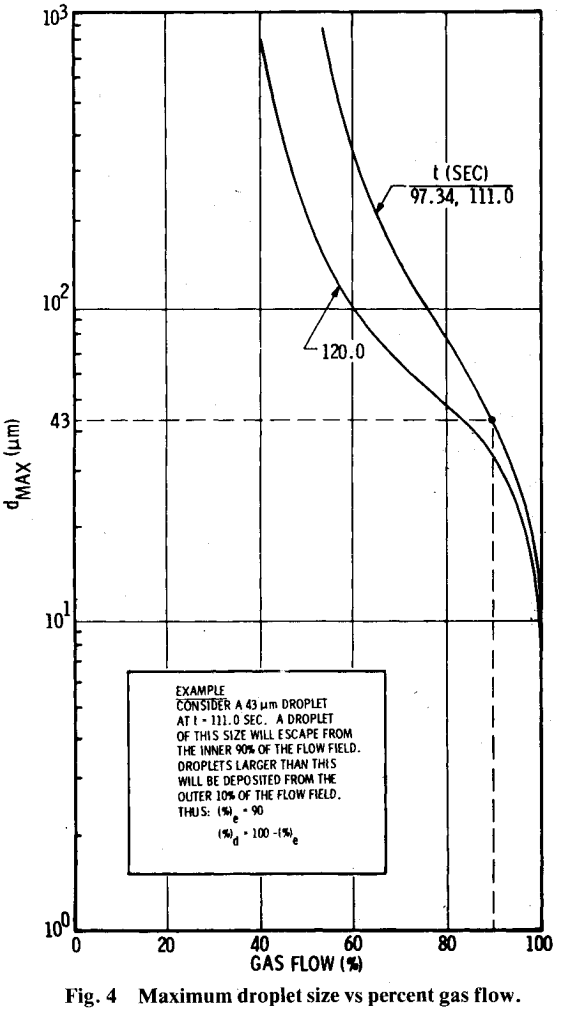

Fig. 4 Maximum droplet size vs percent gas flow.

Table 1 Chamber flow conditions during shutdown QM-2 Motor

t, s	P_O lbf/in.^{2}	T_O, °R	f	$\dot{W}_t$, lbm/s	$\dot{W}_s$, lbm/s
97.34	515.0	6074.9	0.2872	7531.0	2162.9
100.42	485.0	6065.4	0.2871	7097.8	2037.8
111.00	381.0	6027.0	0.2867	5593.5	1603.7
114.43	201.0	5920.3	0.2858	2977.4	850.9
116.16	135.0	5851.0	0.2854	2011.5	574.1
118.27	72.0	5738.0	0.2848	1083.3	308.5
120.00	38.0	5620.0	0.2846	577.7	164.4
122.30	15.0	5445.1	0.2844	186.2	53.0
123.07	13.0	5418.1	0.2843	85.5	24.3

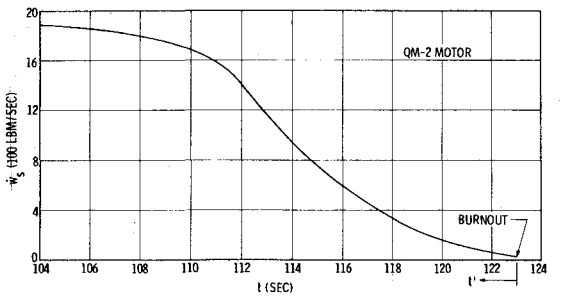

Fig. 5 Total slag flow rate during shutdown.

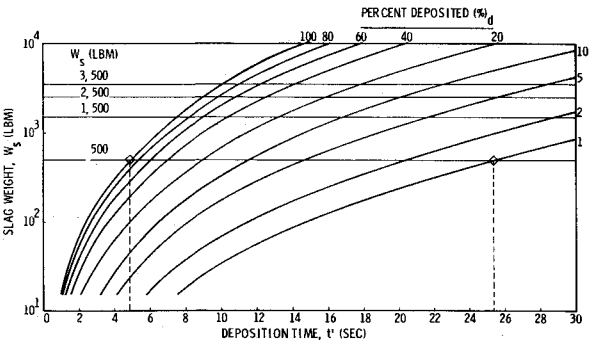

Fig. 6 Weight of slag deposited vs deposition time.

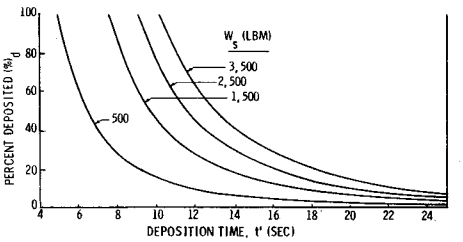

Fig. 7 Percent deposited vs deposition time.

At this point, it was convenient to define a droplet deposition time t' measured backward from the burnout time of 123.07 s, as shown in Fig. 5. Integrating this curve over the deposition time gives the results shown in Fig. 6 for several percentages of slag deposition.

The slag weights shown in Fig. 6 are expected to span the range of slag weights already observed and expected in future SRM static firings. A crossplot at each of these slag weights gives the curves of percent of deposition as a function of deposition time, as shown in Fig. 7. This figure was used in the deposition analysis to determine the percent of the total slag deposited and the time required for deposition.

Droplet Size Distribution

The deposition analysis requires a size distribution of the droplets approaching the nozzle. This distribution was obtained by first taking the experimentalal data of Ref. 1 and extrapolating it down to the chamber pressures of 515.0, 381.0, and 38.0 lbf/in.^{2} corresponding to the SRM burn times of 97.34, 111.0 and 120.0 s, as shown in Fig. 4. The results are shown in Fig. 8 in terms of the droplet volume fraction and the actual droplet diameter. Since the propellant and the combustion conditions within the SRM are different than those for which the experimental data were obtained, the curves of Fig. 8 were nondimensionalized in terms of the minimum droplet diameter at the highest value of SRM chamber pressure (515.0 lbf/in.^{2}) shown. The result is that the minimum, average, and maximum droplet sizes

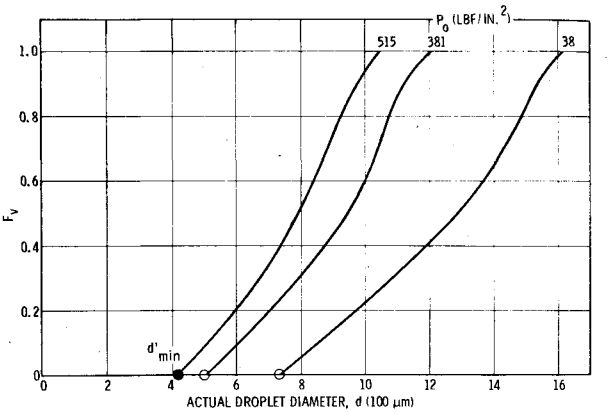

Fig. 8 Volume distribution of droplets.

Table 2 Droplet size coefficients

$d_{min} = a + d'_{min}$ $\quad d_{max} = c \times d'_{min}$
$d_{av} = b \times d'_{min}$ $\quad d'_{min}$ = minimum droplet diameter at maximum pressure ($P_0 = 515.0$ lbf/in.^{2})

t, s	P_0, lbf/in.^{2}	a	b	c
97.34	515.0	1.00	1.83	2.50
111.0	381.0	1.21	2.14	2.87
120.0	38.0	1.74	2.95	3.97

represented by the curves in Fig. 8 can be expressed in terms of a coefficient (a, b, c) times this minimum reference diameter, as shown in Table 2.

The coefficients of Table 2 represent the nondimensionalized distribution of droplets near the burning propellant surface of the SRM during the shutdown period. There is no known experimental information on how these distributions would be altered by droplet collisions and coalescence. It is possible that a program like the one-dimensional three-phase (OD3P) computer program[11] ultimately could be used to determine this effect. In this study, it was assumed that the distributions at the nozzle entrance would be the same as those at the burning propellant surface. This is strongly supported by the work of Crowe and Willoughby,[12] who predicted that droplet collision and coalescence would increase the droplet diameters but not the size distribution. Consequently, the results of Table 2 were used in the deposition analysis.

Deposition Analysis and Results

A procedure was developed which uses the data of Figs. 4 and 7 and Table 2 to clculate in closed form the following quantities concerning deposition:

1) The time (t') required to deposit a given amount of slag and therefore the time (t) into the burn when this deposition starts.

2) The percentage [(%)d] of the total slag in the flowfield which is deposited.

3) The minimum droplet diameter (d'_{min}) during the period of interest or the total slag weight.

With these quantities known, additional information can be obtained. For example, assuming a uniform droplet distribution across the chamber, the portion of the flowfield which contributes the slag will be the annular region adjacent to the motor case wall whose size relative to the total flowfield is the same percentage as that of the total slag deposited. This assumption of uniform droplet distribution is expected to be valid for the large length-to-diameter SRM propellant grain near the end of burn. In addition, once the minimum droplet diameter is known, the size distribution of the deposited droplets can be determined using the coefficients of Table 2.

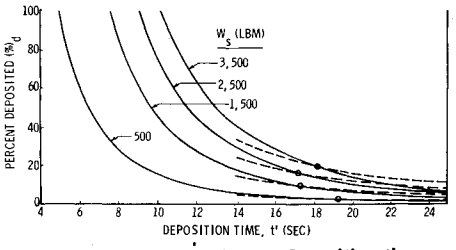

Fig. 9 Percent deposited vs deposition time.

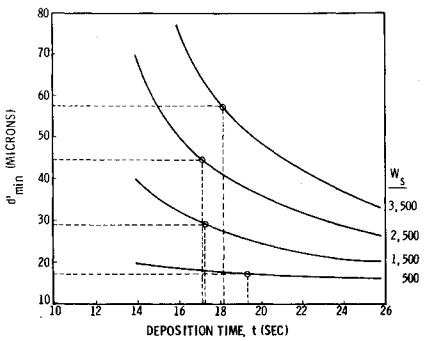

Fig. 10 Minimum droplet size vs deposition time and deposition weight.

The calculation requires that either the minimum droplet diameter or the total slag weight be specified. Since the slag weight is more likely to be known, the procedure described here assumes this to be a known or selected quaantity. A calculation using this procedure is shown below for a static horizontal firing of an SRM over the range of slag weights shown in Figs. 6 and 7.

Procedure

1) Assume a deposition time (t').

2) Determine the burn time (t) when deposition starts ($t = 123.07 - t'$).

3) Determine from Table 1 the chamber pressure P_{O_t} when deposition starts.

4) Determine from Fig. 5 the average slag flow rate ($\dot{w}_{s_{av}}$) during the assumed deposition period.

5) Assume a minimum droplet diameter (d'_{min}) during the period being considered.

6) Calculate the minimum droplet diameter (d_{min}) at the three chamber pressures 38.0, 381.0, and P_{O_t} corresponding to the burn times 120.0, 111.0, and t using the a coefficients of Table 2.

7) At one of the above chamber pressures, set $d_{min} = d_{max}$ in Fig. 4 and determine from this figure the percentage, $(\%)e$, of the gas flowfield from which droplets of this size will escape. Then determine the percentage of the flowfield from which droplets larger than this are deposited. This is $(\%)d = 100 - (\%)e$.

8) Repeat step 7 for each of the remaining chamber pressures. Then determine an average deposition percentage, $(\%)_{d_{av}}$, during the deposition period.

9) Calculate the weight of slag deposited during the deposition period. This is $W_s = t' \times \dot{w}_{s_{av}} \times (\%)_{d_{av}}$.

10) Assume other values of d'_{min} in step 5 and repeat steps 6-9 to get additional values of W_s. This provides a variation of W_s with $(\%)_{d_{av}}$ and d'_{min} for a given deposition time.

11) Repeat steps 1-10 for other deposition times. Results from step 10 are then plotted in the following manner:

a) $(\%)_{d_{av}}$ vs W_s for different deposition times (t').

b) (d'_{min}) vs W_s for different deposition times (t').

12) At each of the four slag weights of Fig. 7, crossplot the data in the plot described in step 11a to obtain a variation of $(\%)_{d_{av}}$ vs t'. Plot these variations onto the results of Fig. 7 as shown in Fig. 9. The intersections of the curves in Fig. 9 provide for each slag weight, the deposition time and the percentage of the slag in the flowfield which is deposited.

13) At each of the four slag weights of Fig. 7, crossplot the data in the plot described in step 11b to obtain a variation of d'_{min} vs t'. These variations are shown plotted in Fig. 10. Using the above-determined deposition times, the minimum droplet diameter during the shutdown can be determined for each of the slag weights.

The results of the above analysis are summarized in Table 3. They show that the deposition time is nearly constant and independent of the slag weight, varying only from 17.2 to 19.3 s. These times are certainly near the end of the motor burn, as postulated at the start of the analysis. The nearly constant deposition times mean of course that the onset times for deposition are nearly the same for all slag weights. The results show that an increase in slag weight from 500 to 3500 lbm is due to the combined effect of a percentage increase from 2.6 to 20.2% in the amount of slag deposited and an increase in the minimum droplet diameter from 14.5 to 57.3 μm. The latter reflects an increase in the size of all droplets deposited when the slag weight increases. The percentage of the droplets deposited also defines the outer percentage of the flowfield from which they originate. For example, for 500 lbm of slag, the deposited droplets come from the outer 2.6% of the flowfield outside of the 97.4% gas flow streamline (Fig. 3). All slag material up to 3500 lbm is extracted from the flowfield outside of the 79.8% gas flow streamline.

The minimum droplet diameters shown in Table 3 along with the coefficients of Table 2 were used to obtain the minimum, average, and maximum droplet diameters of Table 4 at different pressures during the deposition period. The decrease in pressure during the shutdown reveals a rather sizeable increase in the droplet diameters. The average droplet diameter (d_{AV}) shown in the last column of Table 4 is the time-averaged valued of the three average droplet diameter (d_{av}) values during the shutdown. This shows that the average droplet diameter increases from 35.6 μm for 500 lbm of slag to 141.5 μm for 3500 lbm. This is equivalent to a 3.53 μm increase in the average droplet diameter for every 100 lbm increase in deposited slag weight.

Deposition and Accumulation Model

The results of the deposition analysis provided an insight into where the nonescaping droplets would be deposited. As noted, the deposited slag is composed of droplets which were in approximately the outer 20% of the flowfield. The streamlines of Fig. 3 strongly suggest that droplets outside of the 80% gas flow streamline will be deposited on the outer surface of the submerged nozzle. From this, a model was proposed which describes the deposition and accumulation of slag during a static horizontal motor firing, as shown in Fig. 11. When droplets impinge and collect to a certain depth on the upper half of the nozzle, the accumulating molten slag will be acted upon by a shear force due to the adjacent gas flow and a gravitational force. As depth increases the latter will dominate, causing the slag to flow outward to the 90 and 270 deg stations where it leaves the nozzle in the form of drops or thin liquid sheets.

When droplets impinge and collect to some significant depth on the lower half of the nozzle, slag drops may form and fall off the surface. If a drop forms, the force tending to detach it is its weight and the forces tending to prevent such a detachment are the drag imposed by the gas flow directed toward the nozzle surface and the surface tension force around the droplet periphery. Balancing these forces defines a critical droplet size. Calculations of this critical drop size during the shutdown period show that droplets on the order of 0.6 in. diameter may be shedding from the lower nozzle surface near the 90 and 270 deg stations. At the 0 deg station at point 1, the drag force is so great that drops are prevented

Table 3 Results of deposition Analysis

W_s, lbm	t', s	t, s	P_{O_t}, lbf/in.^{2}	$(\%)_{d_{av}}$	d'_{min}, μm
500	19.3	103.77	454.98	2.6	14.5
1500	17.3	105.77	437.07	9.6	29.0
2500	17.2	105.87	436.18	15.9	44.0
3500	18.2	104.87	445.13	20.2	57.3

Table 4 Calculated droplet sizes

W_s, lbm	d'_{min}, μm	P_O, lbf/in.^{2}	d_{min}, μm	d_{av}, μm	d_{max}, μm	d_{AV}, μm
500	14.5	454.98	15.8	28.5	38.7	35.6
		381.0	17.5	31.0	41.6	
		38.0	25.2	42.8	57.6	
1500	29.0	437.07	32.5	58.3	78.7	71.9
		381.0	35.1	62.1	83.2	
		38.0	50.5	85.6	115.1	
2500	44.0	436.18	49.4	88.5	119.6	109.1
		381.0	53.2	94.2	126.3	
		38.0	76.6	129.8	174.7	
3500	57.3	445.13	63.5	114.1	154.3	141.5
		381.0	69.3	122.6	164.5	
		38.0	99.7	169.0	227.5	

from forming. This suggests that slag removal from this region is in the form of a liquid layer flowing along the bottom surface of the nozzle from points 1 to 2, where it leaves the nozzle and impinges on the motor case wall at point 3. From this point, the slag flows forward toward point 4 with an assist from the gas flow within the recirculation region.

III. Application

The results of the deposition analysis were used to investigate the cause of an increased amount of slag produced in the QM-2. A portion of the analysis was repeated for the SRM in flight to determine the effects of flight accelerations on slag deposition.

QM-2

The increase in the amount of slag in the QM-2, as compared with earlier static firings, was apparently due to some phenomena that caused the time-average droplet size to increase from 37.8 to 96.3 μm based upon the calculated values of Table 4. The experimental work by Caveny and Gany[2] indicated that very slight differences in the propellant can result in large differences in the sizes of the agglomerates formed. There were, in fact, some known minor differences between the propellant in the two center segments of this motor and the center segments of the previous five motors. These differences came about because the two center segments of the QM-2 were cast from a different propellant lot. The actual cause of the droplet size increase has not been positively identified; however, it may have been due to the small differences in the chloride and chlorate ion content which were subsequently detected in the two propellant lots.

If the slag increase was due to these propellant differences, then at least this increase must have had its origin in the two center segments. Figure 13 shows the propellant remaining in the QM-2 at approximately the midpoint of the deposition period. The escape zone shown here is the 40% gas flow streamline as determined from the droplet trajectory calculations and is slightly larger than the initial zone (37.5%) determined from a geometrical basis. All droplets within this zone will escape, including all droplets emanating off the propellant remaining in the forward segment. Thus, the approximate 99% of all the slag in the SRM deposited in the nozzle region of the QM-2 motor, and indeed for all SRM, is formed from droplets originating at the propellant surface of the two center segments. This confirms the belief that differences in the propellant in these segments was the cause of the increase in the slag in the QM-2.

The slag formed during the QM-2 firing left enough evidence to make a comparison of its maximum depth with a calculated value of the critical depth. The results of Table 3 were used to determine a deposition start time of 105.9 s. The critical depth, which was calculated to be 26.1 in., was reached at 116.7 s. This meant that the slag remained in the form of a pool for a period of 8.8 s ($t_p = 116.7 - 105.9 - 2.0$). The time at which the critical depth was reached cannot be verified. However, the pool of molten slag left a "high water" mark in the form of solodofoed slag on the motor case wall at approximately 26 in. high. This excellent agreement with prediction gave credence to the pooling model and additional support to the deposition and accumulation model.

SRM in Flight

The effect of flight acceleration on slag deposition was investigated using the maximum axial acceleration of 2.6g during the predicted deposition period. When the droplet trajectory calculations were repeated, the maximum droplet size curves obtained were identical to those of Fig. 4 within the accuracy of reading the droplet impingement points. Since neither the total slag flow rate through the motor nor the droplet size distribution would be expected to change, the amount of slag deposited will not be affected by flight acceleration providing the maximum droplet size does not exceed 80 μm. For larger droplets, the droplet velocity lag would have to be considered in the droplet trajectory calculations. From Table 4, a maximum droplet diameter of 80 μm corresponds to 890 lbm of slag. Thus if this amount is not exceeded in a static firing, one would not expect a larger value had the same firing been for a vehicle in flight. If the quantity of slag in a static firing exceeds this value, a larger value could be expected in flight.

The slag droplets which do not impinge on the nozzle surface but impinge on the motor case wall in the nozzle region apparently coalesce with other deposited droplets to form rivulets and/or thin layers of slag which flow down along the motor case wall. Post-test examinations of the QM-2 after this study was conducted produced ample evidence, in the form of small quantities of solidified slag, to support the above hypothesis of deposition and accumulation both on the nozzle surface and the motor case wall.

Pooling Model

The slag deposition and accumulation model clearly demonstrated that the slag will collect in the base of the motor underneath the nozzle. It was further postulated that as the slag collects there it will form a pool within the confines of the recirculation region, as shown in Fig. 12. It had already been determined that the size of this recirculation region would remain constant during the deposition period; hence, it would remain constant during the accumulation and pooling as well. It was further postulated that the slag is initially constrained from moving forward of the recirculation region by the dynamic pressure of the oncoming gas. However, as its depth increases with time during the shutdown period and the dynamic pressure decreases, a critical depth of the slag is reached when it will start to flow forward into the aft segment of the motor. There is a period of time between the onset of pooling until the critical depth is reached during which the pooled slag may cause damage to the motor case insulation in contact with it. This time period can be determined using the results of the deposition analysis to determine the variation of the slag depth as a function of the time from the start of deposition and an expression for the critical depth.

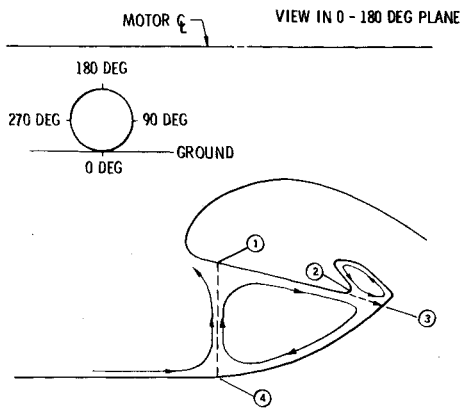

Fig. 11 Slag deposition and accumulation schematic.

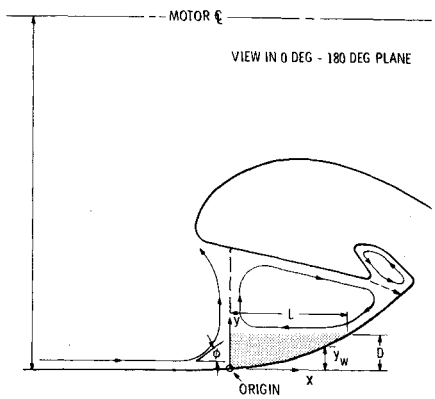

Fig. 12 Slag pooling schematic.

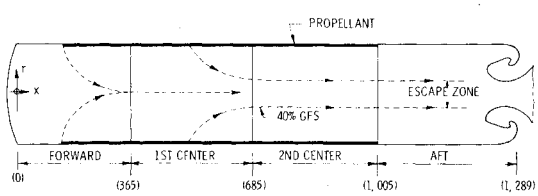

Fig. 13 QM-2 propellant location at approximately the midpoint of the deposition period.

The following procedure was developed for calculating the critical depth, the time into the burn when this depth occurs and time interval that a slag pool exists. It is described below for the pooled slag configuration shown in Fig. 12.

Procedure

1) Determine the variation in slag volume with time into the burn $v = v(t)$, using the following expression:

$$v = (1/\rho_s) \int_t^{t+\Delta t} (\%)_d \dot{w}_s \, dt$$

where t and $(\%)d$ are the time that deposition starts and the percentage of the slag deposited, both obtained from the deposition analysis, and $\dot{w}_s$ is the slag flow rate from Fig. 5.

2) Determine an expression for the volume of the pooled slag in terms of the motor case geometry. The pooled slag occupies a circular segment of angle 2θ in the plane perpendicular to the motor centerline and passing through the origin shown. Its volume can be expressed as

$$v = \tfrac{1}{2}(R - D_{av})\,(2\theta - \sin 2\theta)\,L$$

3) From a polynominal curve fit, $y_w = y_w(x)$, of the motor case wall contour in the recirculation region, determine the average slag depth from

$$D_{av} = (1/L) \int_O^L (D_{max} - y_w)\, dx$$

4) Solve the three equations of steps 1-3 for the three unknowns (v, D_{av}, and D_{max}) at a given value of Δt. From these results, determne the variation in maximum slag depth with the time, $D_{max} = D_{max}(t)$, from start of deposition. This corresponds to an instantaneous pooling of the slag when deposition starts.

5) Correct $D_{max} = D_{max}(t)$ for the delay between the time deposition starts and the time the slag reaches the bottom of the motor case. A delay time (δt) of 2 s was estimated for the SRM. The actual slag depth as a function of time from start of deposition is now expressed as $D = D(t)$.

6) The critical slag depth is calculated as

$$D_c = (1/\rho s)\,(4 + K)\,q_{av}$$

7) With $D = D(t)$ and D_c known, the time (t_c) when the critical depth is reached can be calculated. With t as the time when deposition starts, the time interval that the collected slag is in the form of a pool is $t_p = t_c - t - \delta t$.

The deposition of slag in flight would be expected to be similar to that for a static firing. However, the accumulation and pooling of the slag would be more symmetrical relative to the motor centerline.

IV. Conclusions

An analytical procedure has been developed for calculating specific quantities relating to the deposition and pooling of slag in the Space Shuttle solid rocket motor (SRM). Either the minimum slag droplet size or the deposited slag weight must be specified. For a static horizontal firing where the latter is known, these quantities are the time when deposition starts, the percentage of total slag deposited, the percentage of flowfield contributing slag, the size distribution of deposited droplets, the maximum or critical depth of the pooled slag, and the slag pooling time. Post-test observations of solidified slag on the internal surfaces of these motors support the hypotheses concerning slag deposition, accumulation, and pooling.

The results of a deposition analysis using the developed procedure were used to show that the increased amount of slag in the QM-2 was due to minor differences in the propellant in its two center segments. The same results

demonstrated that flight acceleration will not increase the amount of slag deposited unless the slag weight for a static firing exceeds 890 lbm for some reason; the current average value for all static firings is 681 lbm.

The analytical procedure developed in this study for the SRM should be applicable to other motor configurations, but may be somewhat more complicated for noncylindrical motors and certain grain designs.

References

[1]Gany, A., Caveny, L.H., and Summerfield, M., "Aluminized Solid Propellants Burning in a Rocket Motor Flowfield," *AIAA Journal*, Vol. 16, July 1978, pp. 736-739.

[2]Caveny, L. H. and Gany, A., "Breakup of Al/Al_2O_3 Agglomerates in Accelerating Flowfields," *AIAA Journal*, Vol. 17, Dec. 1979, pp. 1368-1371.

[3]Caveny, L. H. and Gany, A., "Aluminum Combustion Under Rocket Motor Conditions," AGARD Propulsion and Energetics Panel Symposium on Solid Rocket Motor Technology, April 1979.

[4]Landsbaum, E. M., "Formation of Slag," JANNAF Workshop on Acceleration Effects on Space Motors, Feb. 1981.

[5]Eisel, J. L., Brown, B. G., and Price, E. W., "Pressure, Velocity and Geometry Effect on Al_2O_3 Produced During Aluminized Propellant Combustion," *AIAA Journal*, Vol. 13, July 1975, pp. 913-917.

[6]Boraas, S., "Space Shuttle SRM Slag Study," Thiokol Corporation/Wasatch Division, Brigham City, Utah, TWR-12645, Feb. 1980.

[7]Salita, M., "Prediction of Incompressible Viscous Flow Using the SOLA-TC Code," Thiokol Corporation/Wasatch Division, Brigham City, Utah, IOM 2814-81-M122, Sept. 1981.

[8]Hirt, C. W., Nichols, B. D., and Romero, N. C., "SOLA-A Numerical Solution Algorithm for Transient Fluid Flows," Los Alamos Scientific Laboratory, LA-5852 Jan. 1975.

[9]"Space Shuttle SRM Cold Flow Tests, Final Report," Thiokol Corporation/Wasatch Division, Brigham City, Utah, TWR-10604, July 1975.

[10]Gordon, S. and McBride, B. J., "Computer Program for Calculation of Complex Equilibrium Compositions, Rocket Performance, Incident and Reflected Shocks and Chapman-Jouget Detonations," NASA SP 273, 1971.

[11]Hunter, S. C., Cherry, I. S., Waldman, C. H., and Kliegel, J. R., "One-Dimensional Three-Phase Reacting Flow With Mass Transfer Between Phases," KVB Inc., AFRPL-TR-79, Vol I.

[12]Crowe, C. T. and Willoughby, P. G., "A Study of Particle Growth in a Rocket Nozzle," *AIAA Journal*, Vol. 5, July 1967, pp. 1300-1304.